

RESEARCH

Open Access



Synergistic breast cancer therapy with RGD-decorated liposomes co-delivering mir-34a and cisplatin

Hassan Bardania¹, Marzieh Baneshi², Reza Mahmoudi¹, Fatemeh Khosravani³, Farshad Safari³, Bahman Khalvati^{1,4}, Abdollah Poursamad¹ and Mohsen Alipour^{5,6*}

*Correspondence:
mohsenalipoor2013@gmail.com

¹ Cellular and Molecular Research Center, Yasuj University of Medical Sciences, Yasuj, Iran
² Department of Chemistry, Cape Breton University, Sydney, NS B1P 6L2, Canada
³ Student Research Committee, Yasuj University of Medical Sciences, Yasuj, Iran
⁴ Biological Mass Spectrometry Center, Stony Brook Medicine, Stony Brook University, Stony Brook, NY, USA
⁵ Department of Advanced Medical Sciences and Technologies, School of Medicine, Jahrom University of Medical Sciences, Jahrom, Iran
⁶ Department of Biochemistry, School of Medicine, Jahrom University of Medical Sciences, Jahrom, Iran

Abstract

To overcome the drug resistance in MCF7 cancer cells and enhance their sensitivity to cisplatin, a liposomal (Lip) nanocarrier modified by arginine-glycine-aspartic acid (RGD) to co-deliver cisplatin (Cis) and miRNA biomolecule (miR-34a) was investigated. The efficiency of this nanocarrier was evaluated through in vitro and in vivo assays against MCF7 and 4T1 cells, respectively. The in vitro results demonstrated that the miR34a-Cis-Lip-RGD formulation had significantly higher efficiency and also a higher apoptotic effect compared to both miR34a-Cis and miR34a-Cis-Lip (76.24%, 58.29%, and 56.2%, respectively). Additionally, miR34a-Cis-Lip exhibited an overall CI value below 1, indicating a synergistic effect of Cis and miR-34a within the Lip system. The miR34a-Cis-Lip-RGD increased the Bax gene expressions compared to both miR34a-Cis-Lip and Cis-miR34a, possibly due to the integrin receptors on the cells, leading to higher uptake. The efficiency of miR34a-Cis-Lip-RGD in reducing tumor size was significantly higher than Cis-miR34a and miR34a-Cis-Lip. The lower volume of the tumor in the group treated with Cis-miR34a-Lip-RGD is presumed to be attributed to improved cellular uptake facilitated by the RGD modification, which enhances the targeted delivery of the therapeutic payload to cancer cells. The overall weight of the mice in all the groups did not exhibit significant changes. This consistent weight maintenance implies the safety of the designed delivery system for vital organs, indicating that the designed delivery system may offer a promising solution to minimize unwanted side effects associated with conventional cancer treatments.

Keywords: RGD peptide, Liposome, miR-34a, Cisplatin, Combination therapy, MCF7, 4T1

Introduction

Breast cancer is one of the most frequently diagnosed cancers worldwide and remains a leading cause of cancer-related mortality among women. While significant progress has been made in treatment modalities, ranging from surgery and radiation therapy to chemotherapy and hormone therapy, chemotherapy remains a cornerstone of breast cancer treatment. Among the chemotherapeutic agents, cisplatin is widely used due to



© The Author(s) 2024. **Open Access** This article is licensed under a Creative Commons Attribution-NonCommercial-NoDerivatives 4.0 International License, which permits any non-commercial use, sharing, distribution and reproduction in any medium or format, as long as you give appropriate credit to the original author(s) and the source, provide a link to the Creative Commons licence, and indicate if you modified the licensed material. You do not have permission under this licence to share adapted material derived from this article or parts of it. The images or other third party material in this article are included in the article's Creative Commons licence, unless indicated otherwise in a credit line to the material. If material is not included in the article's Creative Commons licence and your intended use is not permitted by statutory regulation or exceeds the permitted use, you will need to obtain permission directly from the copyright holder. To view a copy of this licence, visit <http://creativecommons.org/licenses/by-nc-nd/4.0/>.

its ability to kill cancer cells by causing DNA damage, inhibiting DNA synthesis, and triggering apoptosis (Talebi et al. 2021). However, cisplatin-based therapy has limitations, including drug resistance, non-specific biodistribution, and significant side effects (Gao et al. 2009; Fattal and Bochot 2008). Cisplatin resistance arises from various mechanisms, including decreased drug accumulation within cells, inactivation of the drug through binding to specific proteins, enhanced DNA repair processes, and changes in proteins that regulate apoptosis signaling (Ghosh 2019).

Recent research has highlighted the potential of microRNA (miRNA) as a novel therapeutic strategy for cancer. These small RNA molecules, typically 20–24 nucleotides long and with a double-stranded structure, exhibit significant potential in breast cancer treatment (Seyhan 2011; Uz et al. 2019; Fabian and Sonenberg 2012). They regulate gene expression at the post-transcriptional level by binding to messenger RNA (mRNA) and causing its degradation or translational repression (Davidson and McCray 2011). The bio-production of miRNA begins with the RNA polymerases I and III in the nucleus, followed by processing via Drosha and the DiGeorge critical region 8 (DGCR8) proteins. The resulting biomolecule is then carried to the cytoplasm, where it undergoes additional maturation and establishes an active complex in conjunction with RISC. Subsequently, this complex attaches to mRNA, resulting in its degradation (Gandhi et al. 2014). Through their complementary mRNA sequences, siRNA/miRNA molecules down-regulate specific genes and regulate cell pathways to treat diseases caused by gene misrepresentations (Tiscornia et al. 2003; Judge and Maclachlan 2008). In the context of breast cancer, miRNAs can target key pathways involved in tumor growth, drug resistance, and cell proliferation.

A single miRNA molecule can bind to over a thousand mRNA targets, making it a powerful tool for suppressing tumor growth (Díaz and Vivas-Mejia 2013). For instance, miR-34a, which is typically downregulated in cancer cells, upon administration, can modulate critical tumorigenic factors such as Bcl-2 and P53, which play roles in drug resistance and cancer cell survival (Mansoori et al. 2021; Talebi et al. 2021). By targeting these and other key points, miRNAs can inhibit cancer cell growth and proliferation, making them more susceptible to chemotherapeutic agents (Gandhi et al. 2014).

Despite these promising effects, miRNA-based therapies have some limitations such as low biological stability and the risk of immune system activation (Gao et al. 2009; Fattal and Bochot 2008). Additionally, miRNAs are prone to degradation by nucleases, and their low molecular weight (13 kDa) can lead to rapid clearance via glomerular filtration (Akhtar and Benter 2007; Weinstein and Peer 2010). Although chemical modifications have been explored to improve miRNA stability, there is a continuing need for effective delivery systems that can protect miRNAs from degradation, maintain their bioactivity, and reduce immune system responses (Gandhi et al. 2014).

Combination therapy, involving the co-administration of chemotherapeutic agents and biological molecules like miRNA, has emerged as a promising strategy to enhance treatment efficiency and reduce drug resistance. Through this method, the chemotherapeutic agents target cancer-related signaling pathways. Simultaneously, bio-molecules such as miRNA can significantly enhance the efficiency of chemotherapeutics by down-regulating drug resistance genes (Lehár et al. 2009; Jung and Shin 2011). However, this approach shares some common limitations with conventional chemotherapy such as

the requirement for high drug doses, rapid drug clearance, and low solubility and bio-availability of different compounds (Díaz and Vivas-Mejia 2013). To overcome these challenges, drug delivery systems have been developed not only to safeguard treatment agents, maintain their structure and activity, and enhance chemotherapy effectiveness, but also to minimize their side effects and immune system stimulation (Gandhi et al. 2014; Mansoori et al. 2021).

Liposomes, with their dual-layered phospholipids structure, offer a versatile platform for drug delivery. Their inherent biocompatibility and low-allergenicity make them attractive carriers for both chemical and biological drugs (Schwendener 2007). However, their non-specific delivery can limit efficacy and increase side effects. To enhance targeting, researchers have explored various ligands such as peptides, monoclonal antibodies, transferrin, and vitamins, to guide liposomes to specific tumor sites. These modifications aim to minimize adverse effects associated with the cargo while enhancing cellular uptake through receptor-mediated endocytosis pathway (Bardania et al. 2017). Among these ligands, peptides or peptide mimics have attracted significant attention for their facile synthesis, suitable affinity, and high specificity (Alipour et al. 2020). Notably, the RGD targeting peptide exemplifies this, as it demonstrates a specific affinity for tumor cells and vasculature through a unique complex of $\alpha_v\beta_3$ integrin. This integrin is prominently involved in the angiogenesis of solid tumors and is overexpressed in numerous cancer cells (Rahiminezhad et al. 2022; Ebenhan et al. 2021; Bardania et al. 2019; Khosravi et al. 2022).

Recent studies have highlighted the potential of RGD-conjugated liposomes as a versatile platform for drug delivery, primarily due to their targeted delivery capabilities and enhanced cellular uptake. These liposomes offer a controlled release mechanism, which makes them an attractive choice for various therapeutic applications. A notable example is the use of RGD-modified liposomes for delivering curcumin to MCF-7 breast cancer cells, which demonstrated enhanced therapeutic effects and higher rates of apoptosis compared to non-targeted delivery systems (Mahmoudi et al. 2021a). Another study explored pH-sensitive RGD-modified liposomes loaded with doxorubicin, designed to enhance antitumor activity in lung cancer (Fu et al. 2021a). The pH sensitivity allows for drug release in response to the acidic tumor microenvironment, increasing the specificity and reducing off-target effects.

The adaptability of liposomes in encapsulating various drugs has also made them suitable for mRNA delivery. One study demonstrated the successful co-delivery of Cas9 mRNA and sgRNA using RGD-based liposomes, indicating potential applications in gene therapy (Qin et al. 2022). Furthermore, a study with cRGD-conjugated polyethylene glycol-modified liposomes encapsulating miR-34a showed promising results for targeted transport into MDA-MB-231 breast cancer cells. This targeted delivery significantly increased the accumulation of miR-34a in breast carcinoma cells, highlighting a possible strategy for enhancing the efficacy of miRNA-based therapies.

Given the role of miR-34a in regulating key tumorigenic factors such as Bcl-2 and P53, which act in cisplatin resistance of the cancer cell, in this study, a novel RGD-modified liposomal nanocarrier developed for the co-delivery of cisplatin and miR-34a has been introduced. The focus is on evaluating the nanocarrier's precision in sensitizing MCF7 cancer cells to apoptosis through targeted delivery, leveraging specific tumor tissue

recognition. This tailored liposome aims to lower the resistance threshold of the cells to apoptosis, reprogram gene expression upon internalization in cancer cells, suppress tumor growth, and showcase significant regression of tumor tissue in a mouse model.

Materials and methods

Chemicals

Distearoylphosphatidylcholine (DSPC) was purchased from Avanti Polar (USA). Cholesterol, cisplatin, protamine, 3-[4, 5-dimethylthiazol-2-yl]-2, 5 diphenyl tetrazolium bromide (MTT), were obtained from sigma (Germany). miR-34a (UGGCAGUGUCUU AGCUGGUUGU) was sourced from Bioneer (Seoul, South Korea). Fetal bovine serum (FBS), RPMI1640, and Pen/Strep were acquired from Gibco (USA). Dimethyl sulfoxide, methanol, chloroform, and other materials were obtained from Merck (Germany). The MCF-7 human breast cancer cell line was acquired from the Pasteur Institute of Iran. Dipalmitoyl-GRGDSPA was synthesized by Fmoc chemistry method and its characterization results was published in our previous study (Bardania et al. 2016).

Nanoliposomes preparation

Nanoliposomes (Lips) were formulated using a modified thin-film hydration method (Mahmoudi et al. 2021a, b; Schlich et al. 2017). In this process, DSPC, cholesterol, and dipalmitoyl-GRGDSPA (in a ratio of 7:3:1 mM, respectively) were dissolved in 1 ml of chloroform. Subsequently, the solution was moved to a round-bottom flask and subjected to vacuum drying using a rotary evaporator at 50 °C and 150 rpm, resulting in the formation of a lipid film. For the encapsulation of miR-34a, a mixture of 18 µl of protamine (2 mg ml⁻¹), 140 µl of RNase nuclease-free water, and 24 µl of miRNA was prepared and left at room temperature for 30 min. The resulting lipid film was then hydrated and loaded with 1 ml of 500 µg ml⁻¹ solution of cisplatin and RNA/protamine complex. To make uni-lamellar vesicles, the liposomes were sonicated using a UP400S Ultrasonic processor (Hielscher, Germany) for 3 min with a scheme of pulses and pauses of 5 and 2 s, respectively. The non-encapsulated drugs were removed by centrifugation at 29,000 g for 15 min.

Gel retardation assay

To assess the binding capacity of protamine to nucleic acid, varying amounts of protamine were introduced to 1 µg of single-stranded nucleic acid polymer. The mixtures were then incubated at room temperature for 25 min, followed by agarose gel electrophoresis for 20 min at 80 V. The resulting gel was visualized using UV gel documentation. The intensity of each band was measured using Image J software (version 1.52). A calibration curve was generated to convert the intensity of the non-bonded nucleic acid bands into weight of nucleic acid strands. The remaining DNA in each well was considered as bonded DNA and its percent was calculated according to following formula:

$$\frac{\text{Weight of non - bonded DNA bands} - \text{weight of control sample bands}}{\text{Weight of used DNA in complex}} * 100.$$

The control sample is Wp/Wn of 0, which contained only free nucleic acid strands.

Lips characterization

A 10- μ L aliquot of a diluted Lips sample was placed onto a glow-discharged, carbon-coated grid and analyzed by transmission electron microscopy (TEM) (Philips CM30, Netherlands) for evaluation of the size and morphology of Lips. The size distribution of the Lips was assessed using dynamic light scattering (DLS) (HORIBA SZ-100, HORIBA, Kyoto, Japan). The measurements were conducted at room temperature and repeated in triplicate. Furthermore, the stability of Lips was evaluated by storing them at 4 °C and assessing their size by DLS analysis.

Hemolysis assay

Hemolysis caused by liposomal samples was performed by using a photometric method (Bardania et al. 2019). Blood was drawn from healthy volunteers and placed in heparin tubes. Red blood cells (RBCs) were separated by centrifuging at 1500 \times g for 10 min. After removing the plasma supernatant, the RBCs were washed three times with phosphate-buffered saline (PBS). The RBCs were then re-suspended in 1 ml of PBS to reach a 20% (v/v) concentration and mixed with 0.5 ml of liposomal formulations (200 μ g/ml). This mixture was incubated at 37 °C for 2 h and then centrifuged again at 1500 \times g for 5 min. The hemoglobin released into the supernatant was measured spectrophotometrically at 540 nm. Hemolysis levels in PBS and in 1% Triton X-100 served as controls for spontaneous hemolysis and complete hemolysis, respectively. The percentage of hemolysis was calculated using the formula $(Y-X)/Z \times 100$, where Y is the mean absorbance of the supernatant from RBCs treated with liposomal samples, X is the mean absorbance from RBCs treated with PBS, and Z is the mean absorbance from RBCs treated with 1% Triton X-100.

In vitro cell viability

MCF7 cells were chosen for the in vitro investigation of antitumor effects through the MTT assay. For this purpose, the cells were seeded in 96-well plates at a density of 8×10^3 per well and incubated for 24 h. Subsequently, the cultured cells were treated with different concentrations in separated groups as follows; free cisplatin (Cis), free miR-34a (miR34a), Lips, cisplatin loaded Lips (Cis-Lip), miR-34a loaded Lips (miR34a-Lip), a combination of free cisplatin and free miR-34a (miR34a-Cis), cisplatin and miR-34a-loaded Lips (miR34a-Cis-Lip), RGD-modified cisplatin and miR-34a-loaded Lips (miR34a-Cis-Lip-RGD). After 24-h incubation, 10 μ l of MTT solution (5 mg ml⁻¹) and 90 μ l of DMEM medium were introduced to each well followed by a further 3 h incubation. Finally, the supernatants were replaced with 100 μ l dimethyl sulfoxide (DMSO) and the plates were shaken in darkness for 30 min to dissolve formazan crystals. The optical density (OD) of each well was measured at 545 nm utilizing an ELISA reader (Bio-Tek Instruments Inc., Vermont, USA). The viability rate in each well was calculated in triplicate using the following equation:

$$\text{Cell viability rate} = \frac{\text{OD}_{\text{Sample}}}{\text{OD}_{\text{Control}}} \times 100.$$

Moreover, IC₅₀, the half maximal inhibitory concentration, was estimated for all samples by using Excell software. Furthermore, using the Chou and Talalay method with CompuSyn software (Combosyn Inc., Paramus, NJ, USA) (Chou 2006; Fu et al. 2021b), the combination index (CI) was computed. CI values for Cis and miR-34a, in both free and encapsulated forms, were assessed to identify synergistic, additive, or antagonistic cytotoxic effects based on following equation:

$$CI = (D)_1/(D_x)_1 + (D)_2/(D_x)_2,$$

where (D)₁ and (D)₂ are the concentration of drug 1 and drug 2 in the combination system at the IC_x value, respectively. In addition, (D_x)₁ and (D_x)₂ represent the IC_x value of drug 1 and drug 2 alone, respectively.

Apoptosis study

To assess the apoptosis rate, an Annexin V-FITC Apoptosis Detection Kit (Biolegend, San Diego, CA) was employed. MCF7 cells were treated in different groups as follows: control, Cis, miR34a, miR34a-Cis, Lips, Cis-Lip, miR34a-Lip, miR34a-Cis-Lip, and miR34a-Cis-Lip-RGD at the concentration of 16 µg/ml of Cis and 10 nm of miR34a. Following a 24-h incubation, the supernatants were aspirated, and the cells were washed twice with PBS. The cells were then detached using trypsin and collected by centrifuge. Subsequently, the cells were re-suspended in 500 µl of PBS, after which 5 µl of annexin V and 5 µl of propidium iodide (PI) were added. Subsequently, the stained cells were analyzed using a flow cytometer instrument (Becton Dickinson FACS Calibur flow cytometer).

Real-time PCR mRNA assessment

The mRNA expression of cells treated in the following groups at the concentration of 16 µg/ml of Cis and 10 nm of miR34a was evaluated using HPRT1 as the internal control: Cis, miR34a, Lips, Cis-Lip, miR34a-Lip, miR34a-Cis, miR34a-Cis-Lip, miR34a-Cis-Lip-RGD. Real-time PCR was conducted 24 h after treatment to assess the levels of gene expression associated with apoptosis (Bcl-2 and Bax genes) along with the housekeeping gene internal control (GAPDH). Total RNA was extracted utilizing TRIzol reagent (Invitrogen, Carlsbad, CA), followed by reverse transcription into cDNA (Sinaclon, Tehran, Iran). The synthesized cDNA was subsequently analyzed using real-time PCR on a Rotor-Gene 3000 instrument (Bio-Rad, USA) to quantify the expression of the target

Table 1 Sequences of primers used in the current study

Gene	Primers	Primer sequence	Product size
Bcl-2	Forward	5'-GATTGTGGCCTTCTTTGAG-3'	232
	Reverse	5'-CAAAGTGCAGAGTCTTC-3'	
Bax	Forward	5'-ATGGACGGGTCCGGGAG-3'	455
	Reverse	5'-ATCCAGCCCAACAGCCGC-3'	
GAPDH	Forward	5'-AGGTCGGTGTGAACGGATTG-3'	123
	Reverse	5'-TGTAGACCATGTAGTTGAGGTCA-3'	

genes. The primer sequences are outlined in Table 1. The relative expression of each gene was determined using the $2^{-\Delta Ct}$ method.

In vivo antitumor study

32 BALB/c mice (4 weeks old, female; weighing approximately 18–20 g) were acquired from Pasteur Institute (Tehran, Iran) and divided into 4 groups of 8 mice each (group 1: Cis and miR34a, group 2: miR34a-Cis-Lip, group 3: miR34a-Cis-Lip-RGD). The animals were acclimated in the animal facility of Yasuj University of Medical Sciences for at least 1 week, maintained at a temperature of 24 ± 1 °C and humidity of $55 \pm 5\%$ with unrestricted access to a standard diet and tap water. Approval for the experimental procedures was granted by the local Animal Care and Use Committee (Yasuj University of Medical Sciences). Tumor induction was initiated by subcutaneously injecting 100 μ l of 5×10^6 4T1 cell/ml into BALB/C mice. After a week, the mice were treated every 72 h with injections of (1) miR34a-Cis, (2) miR34a-Cis-Lip, and (3) miR34a-Cis-Lip-RGD (at 10 mg Cis/kg and 1.5 mg/kg miR-34a) for 12 days. Mice weights and tumor sizes were assessed over 2 weeks (Faustino-Rocha et al. 2013; Wadhwa et al. 2013). The volume of subcutaneous tumors was calculated based on following equation:

$$V = L \times W^2 / 2,$$

where L and W were length and width of the tumor, respectively.

Statistical analysis

The results are expressed as the mean \pm SD from three independent experiments, and statistical analysis was conducted using one-way analysis of variance (ANOVA) ($P < 0.05$). These analyses were performed utilizing SPSS software, version 18.

Result and discussion

Lips characterization

The optimization of the protamine/microRNA ratio was conducted through a gel retardation assay, involving the addition of various amounts of protamine to 1 μ g of single-stranded nucleic acid polymer to achieve a stable protamine/microRNA complex. The electrophoretic mobility of free nucleic acid and its complexes at different weight/

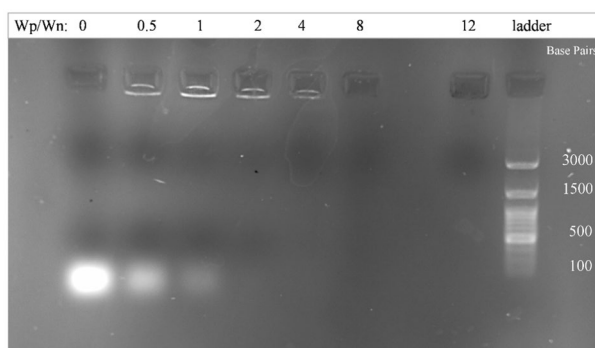


Fig. 1 Electrophoretic mobility of free nucleic acid and its complexes with protamine

weight (w/w) ratios is illustrated in Fig. 1. At a w/w ratio of 0, the nucleic acid exhibited rapid movement, indicating no interaction with the complex. With an increase in the w/w ratio, the nucleic acid's movement slowed down, suggesting a stronger binding affinity with the complex. At w/w ratios of 0.5 and 1, 50% and 90% of the nucleic acid, respectively remained in the well. At w/w ratios of 8 and higher, no signal is detected in the well, presumably due to the complete compaction of the complex and the exclusion of the fluorescent dye. These results align with those of the previous study by Alipour et al. (2023). The successful optimization of the protamine/microRNA ratio in our study corroborates the importance of understanding complex formation dynamics, as demonstrated in the context of Alipour et al.'s work (Alipour et al. 2023), and underscores the potential applications of such optimized complexes in therapeutic interventions for breast cancer and other related conditions.

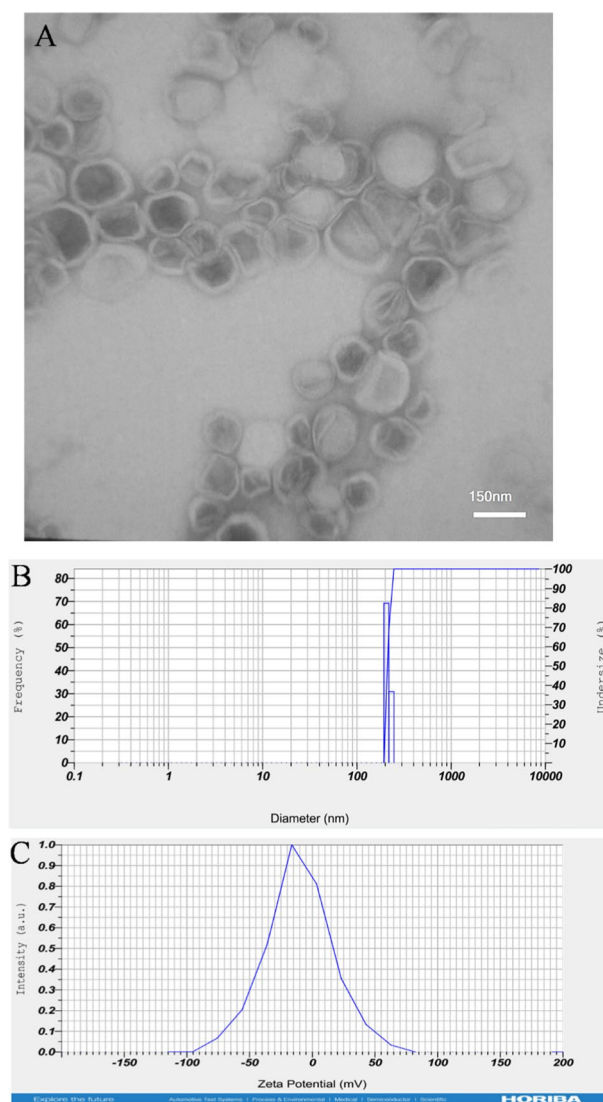
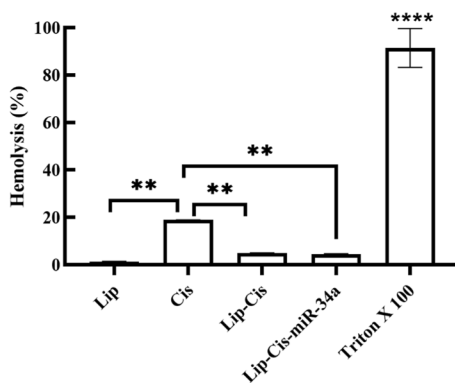


Fig. 2 TEM micrograph (A), size distribution (B) and zeta potential analyzed by DLS (HORIBA SZ-100, HORIBA, Kyoto, Japan) of miR34a-Cis-Lip-RGD

Table 2 DLS analysis of miR34a-Cis-Lip-RGD over a 3-week storage period at 4 °C

Time (week)	Size (nm) + SD
0	213.9 ± 12.3
1	216.1 ± 13
2	218.5 ± 13.3
3	235.7 ± 28.7

**Fig. 3** The effect of Cis and different liposomal formulations on hemolysis blood samples. Data are expressed as mean ± SD of three independent experiments. ***P*-value < 0.01, and *****P*-value < 0.0001 (mean ± SD) indicates significance between the viability of cells treated by different samples

The structure and size of the prepared Lips were examined using TEM and DLS. As illustrated in Fig. 2, the nanoparticles exhibited a spherical shape with a size of approximately 150 nm, while the DLS results indicated a size of around 213 ± 12.3 nm for the Lips. This discrepancy can be attributed to the hydrodynamic radius of the particles in the suspension in the latter case (Souza et al. 2016). The stability assessment of Lips indicated that their size did not undergo significant changes during the period of 3 weeks (Table 2). Zeta potential of Lips was also assessed and was found to be -10.7 ± 1.22 mV (Fig. 2).

Hemolysis assay

The interaction of nanocarriers with blood cells and causing hemolysis has important role for their development and in vivo application. The effect of nanoliposomes on RBC lysis was assessed by hemolysis assay. The results showed that Cis has significant effect of lysis of RBC (Fig 3). Encapsulation of Cis into nanoliposomes significantly decreased their lysis effect compared with free Cis ($P < 0.01$).

In vitro studies

Integrin $\alpha_v\beta_3$ exhibits specific expression characteristics; it is highly expressed on the surface of tumor cells, including MCF-7 cells. Since RGD peptides have strong affinity for the Integrin $\alpha_v\beta_3$, MCF-7 cells were chosen for the assessment of anticancer activity of the prepared carrier (Yan et al. 2020). In Fig. 4 the viability of MCF-7 cells is shown after treatment with Cis and Cis-Lip for various times. These results revealed that Cis has anticancer activity toward the MCF7 cells and its loading on the Lips

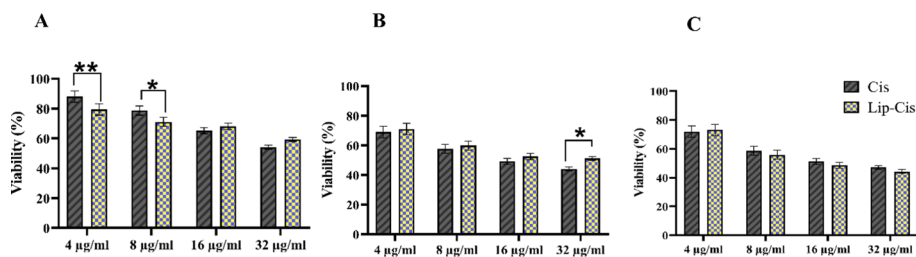


Fig. 4 Viability of MCF-7 cells treated with Cis and Cis-Lip after **A** 24 h, **B** 48 h, and **C** 72 h. Data are expressed as mean \pm SD of three independent experiments. **P*-value < 0.05, and ***P*-value < 0.01 (mean \pm SD) indicates significance between the viability of cells treated by different samples

didn't change its efficiency significantly. These results underscore the potential of the carrier system to preserve and deliver Cis to MCF-7 cells, while the sustained efficiency of the Cis-Lip shows its successful encapsulation and release without compromising its anticancer capabilities. Moreover, the time-dependent response observed in Fig. 4 contributes valuable insights into the kinetics of releasing Cis from Cis-Lip. In addition, IC₅₀ estimation revealed that Lip-Cis, with IC₅₀: 25.48 \pm 1.57 after 72 h treatment, had a greater cytotoxic effect (Table 3). It is possible that Lip-Cis was internalized into cells via endocytosis or other pathways in a time-dependent manner resulted in slowly effect of drug (Huang et al. 2012; Li et al. 2015).

The viability of MCF-7 cells was also assessed after treatment with miR34a, and miR34a-Lip as depicted in Fig. 5. These results revealed that miR34a exerts notable anticancer effects on MCF-7 cells, with its influence being contingent on both concentrations and time which is consistent with other researches (Yang et al. 2018). These results show that the encapsulation of miR34a within the Lip did not introduce a significant alteration in its efficacy, demonstrating that Lip, as the carrier, effectively preserves and delivers miR34a to the MCF-7 cells without compromising its inherent anticancer potency. The consistent efficacy of miR34a, whether free or in encapsulated form, underscores the potential of the Lip formulation to serve as a reliable delivery system for miR34a. Moreover, the IC₅₀ estimated for miR-34a, miR-34a-Lip after 24, 48 and 72 h of treatment was more than 10 nM (data not shown).

Table 3 Comparison of IC₅₀ values (µg/ml) of free form and liposomal form of Cis

Samples	IC ₅₀ for 24 h	IC ₅₀ for 48 h	IC ₅₀ for 72 h
Cis	30.91 \pm 1.42	27.34 \pm 1.21	30.58 \pm 2.19
Lip-Cis	> 32 µg/ml	> 32 µg/ml	25.48 \pm 1.57

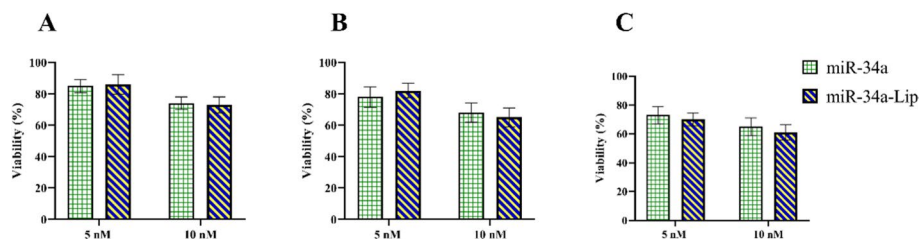


Fig. 5 Viability of MCF-7 cells treated with miR34a and miR34a-Lip after **A** 24 h, **B** 48 h, and **C** 72 h

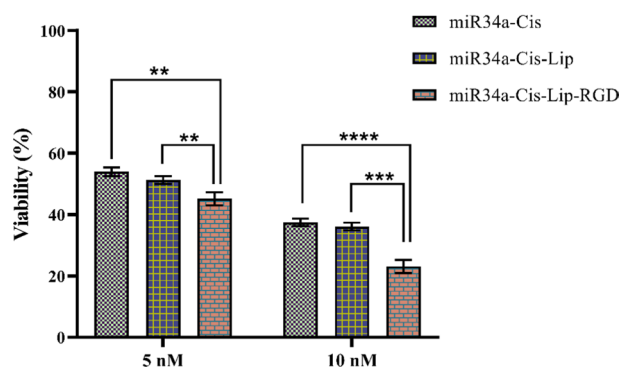


Fig. 6 Viability of MCF-7 cells treated with miR34a-Cis, miR34a-Cis-Lip, and miR34a-Cis-Lip-RGD after 24 h. The concentration of Cis was constant (16 $\mu\text{g}/\text{ml}$). Data are expressed as mean \pm SD of three independent experiments. * P -value < 0.05, ** P -value < 0.01, and **** P -value < 0.001 (mean \pm SD) indicates significance between the viability of cells treated by different samples

Table 4 Comparison of IC 50 values (nM) of miR34a-Cis, miR34a-Cis-Lip, and miR34a-Cis-Lip-RGD

Samples	IC50 for 24 h
miR34a-Cis	6.20 \pm 0.35
miR34a-Cis-Lip	5.41 \pm 0.36
miR34a-Cis-Lip-RGD	3.90 \pm 0.23

The investigation into the anticancer efficacy of miR34a-Cis, miR34a-Cis-Lip, and miR34a-Cis-Lip-RGD on MCF7 cells revealed notable findings, as illustrated in Fig. 6. By comparing cell viability rates between those treated with miR34a-Cis and those treated with miR34a alone or Cis alone, the viability rate of the first group was found to be lower, indicating the enhanced anticancer effect of administering both miR34a and Cis simultaneously.

When comparing the viability rate of cells treated with miR34a-Cis and those treated with miR34a-Cis-Lip, the latter group had a lower viability rate, suggesting that liposomal delivery improves the anticancer efficacy of miR34a and Cis. Furthermore, the comparison of the viability rate of the cells treated with miR34a-Cis-Lip and miR34a-Cis-Lip-RGD demonstrated a significant increase in efficiency when using the RGD-modified formulation. This finding underlines the crucial role of the RGD ligand in targeting the MCF-7 cells, improving the uptake and enhancing the therapeutic impact of this nano-liposomal delivery system.

Upon detailed investigation, it becomes clear that with increased concentration, the anticancer efficacy of miR34a-Cis-Lip-RGD is significantly higher than that of free Cis and non-targeted liposomes. The observed increase in anticancer efficiency, particularly at higher concentrations, not only demonstrates the effectiveness of the nano-liposomal formulation but also underscores the potential of this targeted delivery approach for achieving superior therapeutic outcomes compared to free compounds and untargeted liposomes. Moreover, the results of IC50 estimation confirmed the improvement of miR-34a-Cis-Lip cytotoxicity by modification of their surface by RGD peptide (Table 4).

CompuSyn software was used to evaluate CI values, confirming the synergistic effect of Cis and miR-34a in both miR-34a-Cis-Lip and free forms. miR34a-Cis-Lip

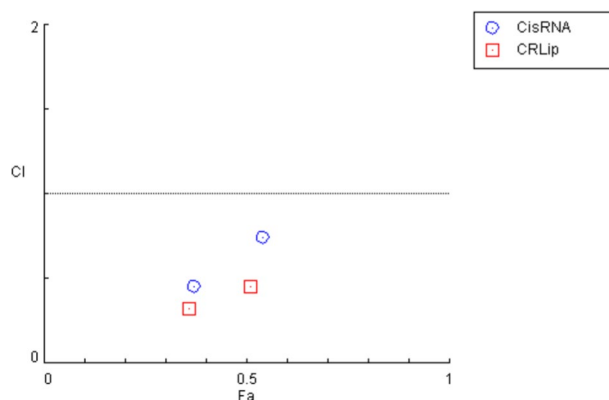


Fig. 7 CI values calculated using Chou and Talalay method. CI: combination index; CisRNA: cisplatin miR-34a; CRLip: cisplatin miR-34a liposome. The values $CI < 1$, $CI = 1$, $CI > 1$ indicate synergism, additive, and antagonism effects, respectively

exhibited an overall CI value below 1, indicating a synergistic effect within the Lip system (Fig. 7). The values $CI < 1$, $CI = 1$, $CI > 1$ indicate synergism, additive, and antagonism effects, respectively.

Apoptosis studies

The apoptotic effect of the designed carrier on MCF7 cells has been evaluated and the results are depicted in Fig. 8. Notably, the incorporation of Cis into Liposomes, demonstrated non-comparable apoptotic effect to free Cis (25.3% vs. 22.6%, respectively). This observation suggests that the liposomal encapsulation of Cis does not compromise its apoptotic efficiency, emphasizing the designed liposomal carrier's ability to maintain the therapeutic impact of the Cis.

In addition, the encapsulation of miR34a into liposomes did not lead to a significant change in apoptotic efficiency compared to free miR34a (25.8% vs. 27.0%, respectively). This result suggests that the liposomal encapsulation does not affect the cellular uptake of the miR34a. This finding aligns with the understanding of the advantages of the liposomal delivery systems in enhancing the bioavailability of the microRNA (Liu et al. 2022).

Comparing the apoptotic effect of miR34a-Cis with the groups treated with Cis alone and miR34a alone, it was found that miR34a-Cis induced a higher rate of apoptosis (56.2%, 25.3%, and 30.8%, respectively), confirming the enhanced apoptotic effect of administering both miR34a and Cis simultaneously.

Moreover, the miR34a-Cis-Lip-RGD exhibited a notably higher apoptotic effect compared to both miR34a-Cis and miR34a-Cis-Lip (76.24%, 56.2%, and 58.2%, respectively). This result highlights the synergistic impact of combining miR34a, Cis, and the RGD ligand within the liposomal framework, resulting in a highly potent apoptotic response. Furthermore, the higher apoptotic efficiency of miR34a-Cis-Lip-RGD emphasizes the vital role of the RGD ligand in facilitating targeted cellular uptake, enhancing the overall therapeutic impact.

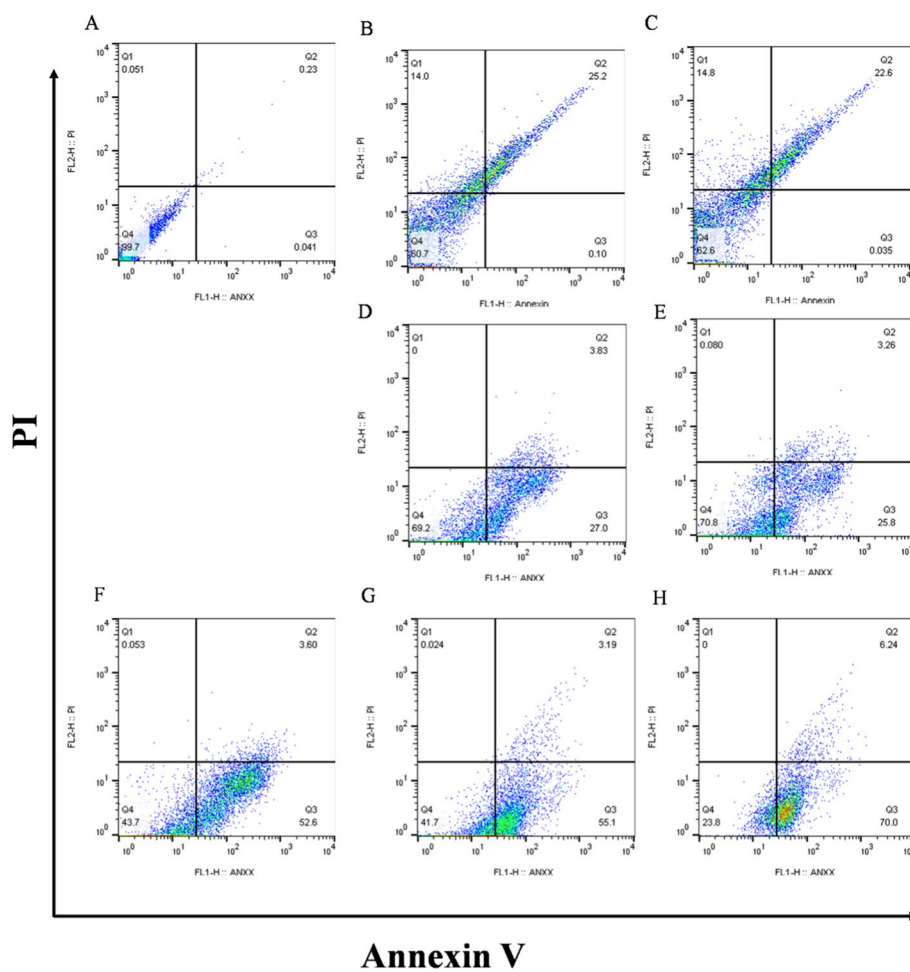


Fig. 8 Flow cytometry analysis of MCF7 cells treated with: **A** control, **B** Cis, **C** Cis-Lip, **D** miR34a, **E** miR34a-Lip, **F** miR34a-Cis, **G** miR34a-Cis-Lip, **H** miR34a-Cis-Lip-RGD

Gene expression analysis

The effect of the designed delivery system on the Bcl-2 and Bax expressions in MCF-7 cells was studied and the results are presented in Fig. 9. These results provide valuable insights into the molecular mechanism underlying apoptosis induced by the designed carrier.

The results highlight the participation of Bcl-2 and Bax genes in the apoptosis induced by the engineered nanoparticles. Notably, in MCF-7 cells treated with miR34a-Lip, there was a significant decrease in Bax expression compared to cells treated with free miR34a. Conversely, the expression of these genes in MCF-7 cells treated with Cis-Lip showed an increase compared to cells treated with free Cis. The loading of both Cis and miR34a onto liposomes (miR34a-Cis-Lip) resulted in a significant enhancement of Bax expression compared to cells treated with miR34a-Cis. Furthermore, the loading of Cis and miR34a onto RGD-modified liposomes (miR34a-Cis-Lip-RGD) exhibited an increased Bax expression compared to both miR34a-Cis-Lip and Cis-miR34a. This enhancement in Bax expression in the presence of RGD

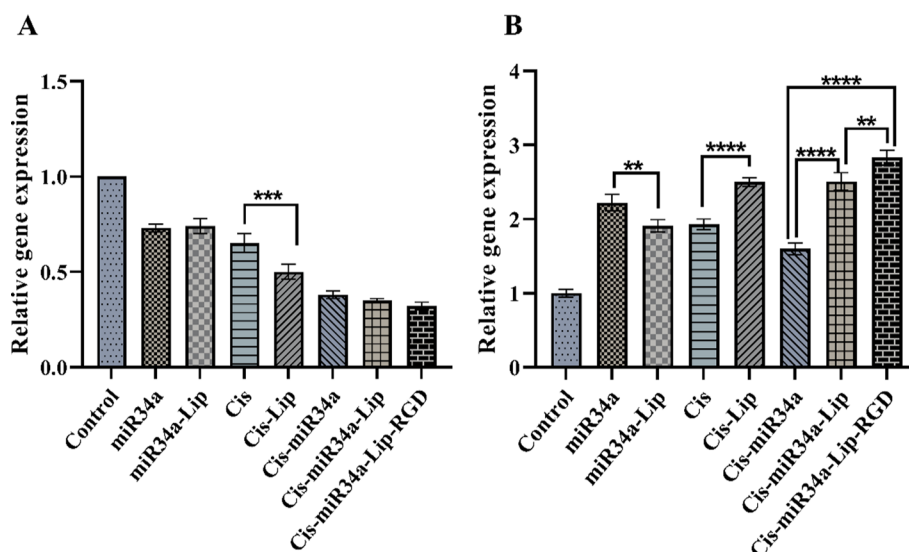


Fig. 9 A Bcl-2 expression, and B Bax expression in MCF-7 cells. The effect of after the treatment with Cis, miR34a, Cis-Lip, miR34a-Lip, miR34a-Cis-Lip, miR34a-Cis-Lip-RGD. Data are expressed as mean \pm SD of three independent experiments. * P -value < 0.05 , ** P -value < 0.01 , and *** P -value < 0.001 (mean \pm SD) indicates significance between the relative gene expression cells treated in different groups

modification suggests a potential role of integrin receptors in facilitating higher nanoparticle uptake, contributing to the amplified apoptotic response.

In terms of Bcl-2 expression, cells treated with miR34a and miR34a-Lip did not show any significant difference, highlighting the stability of Bcl-2 expression with miR34a treatment. However, the loading of Cis onto the Lips significantly decreased Bcl-2 expression in the MCF-7 cells. Although the Bcl-2 expression in cells treated with the miR34a-Cis, miR34a-Cis-Lip, and miR34a-Cis-Lip-RGD can be considered equal, it was significantly decreased compared to cells treated with only Cis or miR34a. It has been demonstrated that silencing the Bcl-2 gene leads to high expression of p53 gene, inducing apoptosis by increasing Bax expression and caspase-3 (Jiang and Milner 2003). Hence, both Cis and miR-34a induce apoptosis by down-regulating the expression of the Bcl-2 gene and upregulating the expression of the Bax gene.

In vivo studies

The antitumor efficiency of Cis-miR34a, Cis-miR34a-Lip, and Cis-miR34a-Lip-RGD was evaluated in vivo, and the results are presented in Fig. 10. Although the tumor size in the control group treated with phosphate saline buffer exhibited continuous growth, all treatment groups demonstrated a reduction in tumor size and volume (Figure S1). After 21 days, the tumor volume of the group treated with Cis-miR34a, Cis-miR34a-Lip, and Cis-miR34a-Lip-RGD were measured to be 9, 6.25, and 2.10 mm², respectively. The significant lower volume of the tumor in the group treated with Cis-miR34a-Lip-RGD is presumed to be attributed to improved cellular uptake facilitated by the RGD modification, which enhances the targeted delivery of the therapeutic payload to cancer cells. However, the overall change in body weight of mice treated by Cis-miR34a-Lip-RGD was significantly higher than the group treated with Cis-miR-34a and Cis-miR-34a-Lip.

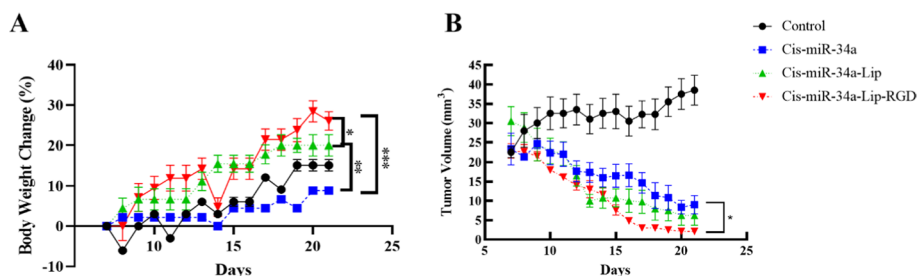


Fig. 10 Antitumor effect of miR34a-Cis, miR34a-Cis-LipP, and miR34a-Cis-Lip-RGD A body weight change of mice, B tumor volume. Data are expressed as mean \pm SD of six independent experiments. * P -value < 0.05; ** P -value < 0.01; and *** P -value < 0.001 (mean \pm SD) indicates significance between body weight change and tumor volume in mice treated by different groups

Conclusion

The focus of this study was on cisplatin resistance in MCF7 cells, which is associated with tumorigenic factors such as Bcl-2 and P53. Since miR34a can regulate these factors, a miR34a-Cis-Lip-RGD formulation was synthesized using the thin-film hydration method. This synthesis resulted in a novel co-delivery system designed for MCF7 cancer treatment. The structural details and release profile of the system were investigated. In vitro cytotoxicity studies using MTT and flow cytometry assays indicated that miR34a-Cis-Lip-RGD exhibits superior anticancer efficiency and apoptotic effects on MCF7 cells compared to the free drug or the single administration of miR34a or Cis attributed to the specific peptide recognition facilitated by the RGD ligand.

The prepared formulation through its peptide recognition mechanism, demonstrated an advantage over the free drug and individual administrations of miR34a or Cis. The specific binding to tumor vasculature, coupled with increased cellular uptake facilitated by the liposomal surface modification with RGD, contributed to its remarkable efficiency in inducing apoptosis and suppressing MCF7 cell viability. Furthermore, the in vivo evaluations against 4T1 cells revealed significant regression in tumor size, highlighting the great potential of the miR34a-Cis-Lip-RGD for breast cancer treatment.

Given the versatility of Cis in treating various cancers and the broad regulatory functions of miR34a, this study suggests that the Cis-miR34a-Lip-RGD carrier could have applications beyond breast cancer treatment. This co-delivery system, which combines the chemotherapeutic properties of Cis with the tumor-suppressing effects of miR34a within a targeted liposomal carrier, holds promise for suppressing MCF7 cancerous cells. Cisplatin is a cornerstone in oncology, used to treat cancers such as lung, ovarian, bladder, and testicular cancer, while miR34a has been implicated in the regulation of key pathways involved in cancer cell growth and survival. This innovative carrier offers the potential for enhanced therapeutic outcomes and reduced side effects, opening the door to further research into its effectiveness across a broader spectrum of cancer types. While our initial focus was on MCF7 cells, to validate the broad-spectrum efficacy of the RGD-modified liposomal co-delivery system, further studies should be conducted to include additional in vitro assays across multiple cancer cell lines (Saraswat et al. 2022; Ozfiliz-Kilbas et al. 2021). Additionally, based on established research, serum stability studies and 3D spheroid assays are vital in understanding the pharmacokinetics and therapeutic efficiency of nanoparticles within a more physiologically relevant tumor

microenvironment (Saraswat et al. 2022, 2023; Saraswat and Patel 2023). Although these assays were beyond the scope of the current study, they have been considered as future research directions.

Acknowledgements

Financial support for this research was provided by Jahrom University of Medical Sciences and Yasuj University of Medical Sciences (Grant ID: 960329).

Author contributions

H.B. performed the experiments, wrote the first draft of manuscript and analyzed the data; M.B. wrote the manuscript, R.M. analyzed the data, F.K., F.S. and B.K. performed the experiments, A.P. wrote and revised the final manuscript, M.A. designed the experiments, and wrote the manuscript. All authors read and approved the manuscript and all data were generated in-house and that no paper mill was used.

Funding

The author(s) disclosed receipt of the following financial support for the research, authorship, and/or publication of this article: This work was financially supported by Jahrom University of Medical Sciences and Yasuj University of Medical Sciences.

Availability of data and materials

No datasets were generated or analysed during the current study.

Declarations

Ethics approval and consent to participate

We received full approval for this study from the Ethics Committee of Jahrom University of Medical Sciences and Yasuj University of Medical Sciences (Approval ID: IR.JUMS.REC.1398.062 and IR.YUMS.REC.1397.145, respectively).

Competing interests

The authors declare no competing interests.

Received: 27 December 2023 Accepted: 14 November 2024

Published online: 22 November 2024

References

- Akhtar S, Benter IF (2007) Nonviral delivery of synthetic siRNAs in vivo. *J Clin Investig* 117(12):3623–3632
- Alipour M, Baneshi M, Hosseinkhani S, Mahmoudi R, Jabari Arabzadeh A, Akrami M et al (2020) Recent progress in biomedical applications of RGD-based ligand: from precise cancer theranostics to biomaterial engineering: a systematic review. *J Biomed Mater Res, Part A* 108(4):839–850
- Alipour M, Sheikhnejad R, Fouani MH, Bardania H, Hosseinkhani S (2023) DNAi-peptide nano-hybrid smart particles target BCL-2 oncogene and induce apoptosis in breast cancer cells. *Biomed Pharmacother* 166:115299
- Bardania H, Shojaosadati SA, Kobarfard F, Dorkoosh F (2016) Optimization of RGD-modified nano-liposomes encapsulating eptifibatide. *Iran J Biotechnol* 14(2):33
- Bardania H, Tarvidipour S, Dorkoosh F (2017) Liposome-targeted delivery for highly potent drugs. *Artif Cells Nanomed Biotechnol* 45(8):1478–1489
- Bardania H, Shojaosadati SA, Kobarfard F, Morshedi D, Aliakbari F, Tahoori MT et al (2019) RGD-modified nano-liposomes encapsulated eptifibatide with proper hemocompatibility and cytotoxicity effect. *Iran J Biotechnol* 17(2):8
- Chou T-C (2006) Theoretical basis, experimental design, and computerized simulation of synergism and antagonism in drug combination studies. *Pharmacol Rev* 58(3):621–681
- Davidson BL, McCray PB (2011) Current prospects for RNA interference-based therapies. *Nat Rev Genet* 12(5):329–340
- Díaz MR, Vivas-Mejía PE (2013) Nanoparticles as drug delivery systems in cancer medicine: emphasis on RNAi-containing nanoliposomes. *Pharmaceuticals* 6(11):1361–1380
- Ebenhan T, Kleynhans J, Zeevaart JR, Jeong JM, Sathekge M (2021) Non-oncological applications of RGD-based single-photon emission tomography and positron emission tomography agents. *Eur J Nucl Med Mol Imaging* 48(5):1414–1433
- Fabian MR, Sonenberg N (2012) The mechanics of miRNA-mediated gene silencing: a look under the hood of miRISC. *Nat Struct Mol Biol* 19(6):586–593
- Fattal E, Bochet A (2008) State of the art and perspectives for the delivery of antisense oligonucleotides and siRNA by polymeric nanocarriers. *Int J Pharm* 364(2):237–248
- Faustino-Rocha A, Oliveira PA, Pinho-Oliveira J, Teixeira-Guedes C, Soares-Maia R, Da Costa RG et al (2013) Estimation of rat mammary tumor volume using caliper and ultrasonography measurements. *Lab Anim* 42(6):217–224
- Fu S, Zhao Y, Sun J, Yang T, Zhi D, Zhang E et al (2021a) Integrin $\alpha v \beta 3$ -targeted liposomal drug delivery system for enhanced lung cancer therapy. *Colloids Surf, B* 201:111623
- Fu Y, Saraswat A, Wei Z, Agrawal MY, Dukhande VV, Reznik SE et al (2021b) Development of dual ARV-825 and nintedanib-loaded PEGylated nano-liposomes for synergistic efficacy in vemurafenib-resistant melanoma. *Pharmaceutics* 13(7):1005
- Gandhi NS, Tekade RK, Chougule MB (2014) Nanocarrier mediated delivery of siRNA/miRNA in combination with chemotherapeutic agents for cancer therapy: current progress and advances. *J Control Release* 194:238–256

- Gao S, Dagnaes-Hansen F, Nielsen EJB, Wengel J, Besenbacher F, Howard KA et al (2009) The effect of chemical modification and nanoparticle formulation on stability and biodistribution of siRNA in mice. *Mol Ther* 17(7):1225–1233
- Ghosh S (2019) Cisplatin: the first metal based anticancer drug. *Bioorg Chem* 88:102925
- Huang F-y, Mei W-l, Li Y-n, Tan G-h, Dai H-f, Guo J-h et al (2012) The antitumor activities induced by pegylated liposomal cytochalasin D in murine models. *Eur J Cancer* 48(14):2260–2269
- Jiang M, Milner J (2003) Bcl-2 constitutively suppresses p53-dependent apoptosis in colorectal cancer cells. *Genes Dev* 17(7):832–837
- Judge A, Maclachlan I (2008) Overcoming the innate immune response to small interfering RNA. *Hum Gene Ther* 19(2):111–124
- Jung HS, Shin YK (2011) The potential RNAi-based combination therapeutics. *Arch Pharmacol Res* 34(1):1–2
- Khosravani F, Mir H, Mirzaei A, Kobarfard F, Bardania H, Hosseini E (2022) Arsenic trioxide and Erlotinib loaded in RGD-modified nanoliposomes for targeted combination delivery to PC3 and PANC-1 cell lines. *Biotechnol Appl Biochem* 70:811
- Lehár J, Krueger AS, Avery W, Heilbut AM, Johansen LM, Price ER et al (2009) Synergistic drug combinations tend to improve therapeutically relevant selectivity. *Nat Biotechnol* 27(7):659–666
- Li Y, Liu R, Yang J, Shi Y, Ma G, Zhang Z et al (2015) Enhanced retention and anti-tumor efficacy of liposomes by changing their cellular uptake and pharmacokinetics behavior. *Biomaterials* 41:1–14
- Liu P, Chen G, Zhang J (2022) A review of liposomes as a drug delivery system: current status of approved products, regulatory environments, and future perspectives. *Molecules* 27(4):1372
- Mahmoudi R, Ashraf Mirahmadi-Babaheidri S, Delaviz H, Fouani MH, Alipour M, Jafari Barmak M et al (2021a) RGD peptide-mediated liposomal curcumin targeted delivery to breast cancer cells. *J Biomater Appl* 35(7):743–753
- Mahmoudi R, Hassandokht F, Ardakani MT, Karimi B, Roustazadeh A, Tarvirdipour S et al (2021b) Intercalation of curcumin into liposomal chemotherapeutic agent augments apoptosis in breast cancer cells. *J Biomater Appl* 35(8):1005–1018
- Mansoori B, Silvestris N, Mohammadi A, Khaze V, Baghban E, Mokhtarzadeh A et al (2021) miR-34a and miR-200c have an additive tumor-suppressive effect on breast cancer cells and patient prognosis. *Genes* 12(2):267
- Ozfiliz-Kilbas P, Sonmez O, Obakan-Yerlikaya P, Coker-Gurkan A, Palavan-Ünsal N, Uysal-Onganer P et al (2021) In Vitro investigations of miR-33a expression in estrogen receptor-targeting therapies in breast cancer cells. *Cancers* 13(21):5322
- Qin J, Xue L, Gong N, Zhang H, Shepherd SJ, Haley RM et al (2022) RGD peptide-based lipids for targeted mRNA delivery and gene editing applications. *RSC Adv* 12(39):25397–25404
- Rahiminezhad Z, Tamaddon A, Dehshahri A, Borandeh S, Abolmaali SS, Najafi H et al (2022) PLGA-graphene quantum dot nanocomposites targeted against $\alpha\text{v}\beta\text{3}$ integrin receptor for sorafenib delivery in angiogenesis. *Biomater Adv* 137:212851
- Saraswat A, Patel K (2023) Delineating effect of headgroup and preparation method on transfection versus toxicity of DNA-loaded lipid nanocarriers. *Nanomedicine* 18(26):1921–1940
- Saraswat A, Vemana HP, Dukhande VV, Patel K (2022) Galactose-decorated liver tumor-specific nanoliposomes incorporating selective BRD4-targeted PROTAC for hepatocellular carcinoma therapy. *Heliyon*. 8(1):e08702
- Saraswat A, Vartak R, Hegazy R, Fu Y, Rao TJR, Billack B et al (2023) Oral lipid nanocomplex of BRD4 PROTAC targeting chimera and vemurafenib for drug-resistant malignant melanoma. *Biomed Pharmacother* 168:115754
- Schlich M, Longhena F, Faustini G, O'Driscoll CM, Sinico C, Fadda AM et al (2017) Anionic liposomes for small interfering ribonucleic acid (siRNA) delivery to primary neuronal cells: evaluation of alpha-synuclein knockdown efficacy. *Nano Res* 10:3496–3508
- Schwendener RA. Liposomes in biology and medicine. *Bio-Applications of Nanoparticles*. 2007:117–28.
- Seyhan AA (2011) RNAi: a potential new class of therapeutic for human genetic disease. *Hum Genet* 130(5):583–605
- Souza TG, Ciminelli VS, Mohallem NDS, editors. A comparison of TEM and DLS methods to characterize size distribution of ceramic nanoparticles. *Journal of physics: conference series*; 2016: IOP Publishing.
- Talebi M, Talebi M, Kakouri E, Farkhondeh T, Pourbagher-Shahri AM, Tarantilis PA et al (2021) Tantalizing role of p53 molecular pathways and its coherent medications in neurodegenerative diseases. *Int J Biol Macromol* 172:93–103
- Tiscornia G, Singer O, Ikawa M, Verma IM (2003) A general method for gene knockdown in mice by using lentiviral vectors expressing small interfering RNA. *Proc Natl Acad Sci* 100(4):1844–1848
- Uz M, Kalaga M, Pothuraju R, Ju J, Junker WM, Batra SK et al (2019) Dual delivery nanoscale device for miR-345 and gemcitabine co-delivery to treat pancreatic cancer. *J Control Release* 294:237–246
- Wadhwa R, Singh R, Gao R, Shah N, Widodo N, Nakamoto T et al (2013) Water extract of Ashwagandha leaves has anticancer activity: identification of an active component and its mechanism of action. *PLoS ONE* 8(10):e77189
- Weinstein S, Peer D (2010) RNAi nanomedicines: challenges and opportunities within the immune system. *Nanotechnology* 21(23):232001
- Yan H, You Y, Li X, Liu L, Guo F, Zhang Q et al (2020) Preparation of RGD peptide/folate acid double-targeted mesoporous silica nanoparticles and its application in human breast cancer MCF-7 cells. *Front Pharmacol* 11:898
- Yang D, Fa M, Gao L, Zhao R, Luo Y, Yao X (2018) The effect of DNA on the oxidase activity of nanoceria with different morphologies. *Nanotechnology* 29(38):385101

Publisher's Note

Springer Nature remains neutral with regard to jurisdictional claims in published maps and institutional affiliations.